



HAL
open science

Cu depletion on Cu(In,Ga)Se 2 surfaces investigated by chemical engineering: An x-ray photoelectron spectroscopy approach

Anais Loubat, Solène Béchu, Muriel Bouttemy, Jackie Vigneron, Daniel Lincot, Jean-Francois Guillemoles, Arnaud Etcheberry

► To cite this version:

Anais Loubat, Solène Béchu, Muriel Bouttemy, Jackie Vigneron, Daniel Lincot, et al.. Cu depletion on Cu(In,Ga)Se 2 surfaces investigated by chemical engineering: An x-ray photoelectron spectroscopy approach. *Journal of Vacuum Science & Technology A*, 2019, 37 (4), 10.1116/1.5097353. hal-02321990

HAL Id: hal-02321990

<https://hal.science/hal-02321990v1>

Submitted on 3 Nov 2019

HAL is a multi-disciplinary open access archive for the deposit and dissemination of scientific research documents, whether they are published or not. The documents may come from teaching and research institutions in France or abroad, or from public or private research centers.

L'archive ouverte pluridisciplinaire **HAL**, est destinée au dépôt et à la diffusion de documents scientifiques de niveau recherche, publiés ou non, émanant des établissements d'enseignement et de recherche français ou étrangers, des laboratoires publics ou privés.

Cu depletion on Cu(In,Ga)Se₂ surfaces investigated by chemical engineering: An x-ray photoelectron spectroscopy approach

Anais Loubat, Solène Béchu, Muriel Bouttemy, Jackie Vigneron, Daniel Lincot, Jean-François Guillemoles, and Arnaud Etcheberry

Citation: *Journal of Vacuum Science & Technology A* **37**, 041201 (2019); doi: 10.1116/1.5097353

View online: <https://doi.org/10.1116/1.5097353>

View Table of Contents: <https://avs.scitation.org/toc/jva/37/4>

Published by the [American Vacuum Society](#)

ARTICLES YOU MAY BE INTERESTED IN

Surface energy engineering for LiTaO₃ and α -quartz SiO₂ for low temperature (<220 °C) wafer bonding

Journal of Vacuum Science & Technology A **37**, 041101 (2019); <https://doi.org/10.1116/1.5095157>

Comparative operando XPS studies of quasi-Fermi level splitting and open-circuit voltage in CZTSe/CdS and CIGS/CdS junctions and device structures

Journal of Vacuum Science & Technology A **37**, 031202 (2019); <https://doi.org/10.1116/1.5090345>

In situ investigation of as grown Cu(In,Ga)Se₂ thin films by means of photoemission spectroscopy

Journal of Vacuum Science & Technology A **37**, 031510 (2019); <https://doi.org/10.1116/1.5089412>

Facile benchtop reactor design using dendrimer-templating technology for the fabrication of polyethyleneimine-coated CuO nanoparticles on the gram scale


Journal of Vacuum Science & Technology A **37**, 041402 (2019); <https://doi.org/10.1116/1.5089593>

Aluminum tri-isopropoxide as an alternative precursor for atomic layer deposition of aluminum oxide thin films

Journal of Vacuum Science & Technology A **37**, 040901 (2019); <https://doi.org/10.1116/1.5093402>

Commissioning of vacuum system for SuperKEKB positron damping ring

Journal of Vacuum Science & Technology A **37**, 041601 (2019); <https://doi.org/10.1116/1.5092956>



NEW

AVS Quantum Science
A high impact interdisciplinary journal for **ALL** quantum science

ACCEPTING SUBMISSIONS

The banner features the AVS logo, the AIP Publishing logo, and a collection of quantum science icons including a triangle with a circle, a cat face, a brain, a signal waveform, and an atom symbol.



Cu depletion on Cu(In,Ga)Se₂ surfaces investigated by chemical engineering: An x-ray photoelectron spectroscopy approach

Anais Loubat,^{1,2} Solène Béchu,^{1,2,a)} Muriel Bouttemy,^{1,2} Jackie Vigneron,^{1,2} Daniel Lincot,^{1,3} Jean-François Guillemoles,^{1,3} and Arnaud Etcheberry^{1,2}

¹Institut Photovoltaïque d'Île-de-France (IPVF), 30 Route Départementale 128, 91120 Palaiseau, France

²Institut Lavoisier de Versailles (ILV UMR 8180), UVSQ—CNRS, 45 avenue des États-Unis, 78035 Versailles, France

³CNRS, Institut Photovoltaïque d'Île de France (IPVF), UMR 9006, 30 RD 128, 91120 Palaiseau, France

(Received 25 March 2019; accepted 17 June 2019; published 8 July 2019)

Photovoltaic cells based on CIGS [Cu(In,Ga)Se₂] absorber technology are among the most efficient thin film solar cells and already an industrial reality. Room for improvement is still possible in the manufacturing process to approach the theoretical ultimate efficiency. This not only requires an optimal absorber material but also the control of the CIGS interface chemistry, especially at the front side with the buffer layer which represents one of the main challenges. In this paper, thanks to x-ray photoelectron spectroscopy (XPS) analysis, the CIGS surface chemical composition is studied after acid (HCl) and basic (KCN) samples dipping. Both are regularly employed to prepare CIGS surfaces. XPS monitoring of the surface composition evolution under air aging at an ambient atmosphere and over a period of 120 days is presented, bringing fundamental information about the surface oxidation trends. If the HCl treatment gives a remarkable deoxidation state for the CIGS surface, it also yields a slightly Se enriched surface indicating the presence of a Cu_{2-x}Se binary side phase, which is totally removed, as expected, by the KCN process. The present comparative study based on intentional air aging of starting HCl and KCN treated surfaces sheds light on the reorganization mechanism of this I-III-VI quaternary compound toward oxidation of clean CIGS surfaces, in ambient conditions. The oxidation process occurs concomitantly with an Na migration toward the surface, with soda-lime glass at the back contact, acting as a nonlimiting supply, asking the question of a surface mechanistic correlation during the CIGS surface oxidation. *Published by the AVS.* <https://doi.org/10.1116/1.5097353>

I. INTRODUCTION

Photovoltaic (PV) cells based on CIGS [Cu(In_xGa_{1-x})Se₂] absorber on the conventional soda-lime substrate is a mature technology, meeting a worldwide interest as manufacturing up-scaling is compatible with the current high-efficiency rate and competitive production costs.¹⁻³ Indeed, CIGS is one of the highest efficiency, low cost, polycrystalline type of solar cells with 22.9%⁴ lab efficiencies and 19.7%⁵ at 1 ft² size minimodule efficiency.^{3,6} To approach the theoretical ultimate efficiency, there is still room for improvement in the manufacturing process,¹ considering the optimization of the absorber material itself and the control of its back and front interfaces properties. A main challenge concerns the absorber/buffer layer interface issue. Indeed, the CIGS surface chemistry influences the buffer layer deposition process, especially on the band alignment at the front side and, therefore, on the final cell efficiency.

In this context, many challenges should emerge to go over the present cells performance and address an enlarged economic market, involving innovative cells architecture. Several lines of research are under consideration, such as the replacement of the CdS buffer layer by new compounds (ZnS, InS_x, etc.) to optimize band alignment,⁷ thinner absorbers to be cost effective without reducing conversion efficiencies,^{8,9} and new

orientation such as CIGS deposition on flexible polyimide¹⁰ or a metallic substrate to increase adaptability to market.¹¹ To achieve such goals, a deep knowledge of the CIGS surface chemical state at its front interface is a key point to be addressed. Indeed, the surface physicochemical properties have to be adapted to the different constraints arising from the technological evolutions (temperature, substrate flexibility, adherence, alkali incorporation, etc.) while maintaining device efficiency, process yield, and long term device stability. This is especially challenging for CIGS, composed of four elements: Cu, In, Ga, and Se, to which Na and ambient oxygen must be added in the global chemical diagnostic. Therefore, possible presence of different oxidized and side compounds (binaries, ternaries and more) and modifications of the physicochemical properties are induced. Finally, although the CIGS structure is derived from the zinc blende one, as for many of the semiconductors used for optoelectronic applications (III-V's, II-VI's), it tends to be more ionic in nature and, more outstandingly, the valence band is mostly formed by antibonding Cu-d and Se-p states.¹² As a consequence, copper vacancies tend to easily form in this system, with the consequence that copper and selenium containing compounds are inclined to display stoichiometric deviations toward the Cu-poor side. Another consequence of this weak bonding is the facilitated diffusion of Cu in the system.¹³ Thermodynamics is one of the first tools which can help understanding these entire phenomena. Indeed, previous

^{a)}Electronic mail: solene.bechu@uvsq.fr

studies^{13–15} show that the stability of the various phases depends on the chemical potential of the elements, and, therefore, on the solid initial composition as well as ambient conditions (oxygen partial pressure, temperature). Many studies report on the comprehension of CIGS surface behavior with regard to the chemical treatment employed.^{14,16–20} The scope of our work is to better understand the mechanisms involved in the CIGS surface formation and on their chemical reorganization in the relevant ambient conditions, especially in air, which is also important for corrosion studies of the CIGS.

Deoxidation/reoxidation sequences, performed on the same samples, are used as an internal probe to provide quantitative information about the respective behaviors of the constitutive CIGS elements toward air interaction. Reactivity during oxidation or oxide dissolution can induce very complex modifications in the distribution of the alloy element and therefore can provide a lot of chemical evidence on the behavior of CIGS surfaces at different stages of the PV device fabrication.

In a recent paper,²¹ we investigated the strong chemical evolution of air-aged bare CIGS surfaces submitted to an HCl treatment, where the CIGS was prepared by Zentrum für Sonnenenergie- und Wasserstoff-Forschung (ZSW).²² The observed chemical evolutions were typical of an efficient deoxidation process of the aged CIGS layers. This paper pointed out a high reproducibility of the immediate post-HCl treatment, through reproducible modifications of the x-ray photoelectron spectroscopy (XPS) signatures and also their related compositional parameters. As expected, HCl treatments of oxidized CIGS surfaces provided very reproducible oxide-free final state whatever the oxidation level of the initial surface. The significant composition evolution was summarized via the changes of the CGI $\{=[\text{Cu}]/([\text{Ga}] + [\text{In}])\}$ ratio while the GGI $\{=[\text{Ga}]/([\text{Ga}] + [\text{In}])\}$ stayed almost constant. This observation about the opposite trends between GGI and CGI evolutions allowed a quantitative discussion about the different chemical configurations associated with strongly oxidized or oxide-free surfaces. Compared to the initial situation, the apparent CGI ratio remarkably increased after the HCl treatment. This initial surface evolution was not surprising as the as-grown aged surfaces were oxidized and abnormally Cu-poor, probably due to the aging process. Recovery of a stronger Cu signal was thus expected through an efficient etching step. Then, a very interesting reverse and slow decay of the CGI in time, under a novel air-aging period, was observed, but leading to a different Cu depleted CIGS surface which remained nevertheless richer than the initial aged as-grown one. These observations evidenced very important reactivity specificities, linked to a compositional oscillation, associated with the chemical engineering sequences. The last point of this paper was that the apparent CGI ratio evolution, associated with Cu quantity changes and likely related to Se features for which spectrum interpretations needed consideration on side selenide phases, even on oxide-free samples. So, clearly, with the HCl treatment came also the question about the behavior of side selenide phases inside the deoxidation process.

Using these previous results, we extend here our reflection about CIGS surface chemistry using a comparative and complete

approach based on the HCl treatment, but also on an additional one, which combines a first HCl treatment relayed by a classical KCN treatment. Our objective is to clarify our interrogations about the Cu balance evolution in relation or not with the specific features observed on Se signals. Indeed, these multiple observations must be considered in a global approach of the oxidation process, where the key parameters are still not perfectly understood. For example, considerations about the modifications of Se, In, Ga, and Cu XPS signals, which are obviously linked, are always opened to discussion especially concerning their relative atomic compositional evolution over time, for air-aged as-grown CIGS as for refreshed samples. The present work contributes to the fundamentals of the physicochemistry of the CIGS surface, providing on the same CIGS surface quantitative comparison between HCl and HCl-KCN treatments. We focus our discussion on the comparative study of CGI ratios evolution determined by high energy resolution spectra interpretation. Moreover, aging sequences of freshly treated surfaces are used as tools to collect complementary information about the CIGS reactivity. Our goal is to separate evolutions associated with the apparition and loss of oxide phases with possible selenide ones. Two ways have been investigated and performed in parallel to provide a quantitative comparison: one, associated with HCl treatment, focuses on the elimination of oxide phases,^{21,23} and the other, associated with the KCN treatment, prolongs the elimination of the oxide phase by the side selenide ones.^{18,23–25} Finally, a combination of HCl and then KCN treatment, expected as the most efficient procedure to reach a well-defined CIGS surface, is discussed. Then, the reoxidation phase of the two kinds of oxide-free surface is investigated by comparing their surfaces evolution with the ones of similarly treated samples kept during the same time under an ultrahigh vacuum (UHV) condition. This confrontation brings key features to understand CIGS surface reactivity origin and address essential technological issues.

II. EXPERIMENT

A. Materials and chemical engineering of CIGS surfaces

This study is performed on the same batch of as-grown aged CIGS layers. They were stored without any capping toward air aging interaction until their use for the present work. The CIGS samples were supplied by ZSW, Germany.²²

CIGS was deposited by coevaporation on Mo (600 nm)/glass (3 mm) substrates. The CIGS layers were provided with optimal GGI = $[\text{Ga}]/([\text{Ga}] + [\text{In}])$ and CGI = $[\text{Cu}]/([\text{Ga}] + [\text{In}])$ bulk ratios typically expected in the range from 0.30 to 0.35 and around 0.80, respectively, and a thickness of 2.1 μm . The initial large area sample was divided into several equivalent area pieces in order to study a batch of comparable materials when exposed in parallel to different chemical treatments or atmosphere, and following the same aging conditions after.

The wet chemical treatments based on acid ($\text{pH} < 1$) or basic ($\text{pH} > 10$) solutions are performed using HCl (1.0M, 5 min) for the acid one^{21,23} and KCN (1.0M, 5 min) for the basic one.^{18,23–25} After soaking, samples are first rinsed in

ultrapure water (18.2 MΩ) and then dried under nitrogen (N₂) flux. For the study of the fresh etched surfaces, they are stored in a Thermo Electron transfer vessel compatible with the entry-lock of the K-Alpha XPS spectrometer, maintaining them under low vacuum conditions (15 min, $\sim 10^{-3}$ Pa) until the introduction chamber. Note that the HCl-KCN coupling process consists of a two steps immersion protocol: the HCl treatment is followed, after an intermediate rinsing step of 2 min, by the KCN one. For the air reactivity study, treated samples are initially characterized by XPS and then stored in a glass vessel filled with laboratory air for different durations. This aging is performed at constant temperature (21 °C) and humidity (55%) and only intermittently interrupted to perform the XPS analysis at defined intervals.

B. Surface characterization by XPS

Chemical evolution of the CIGS surface stability is investigated by systematic XPS analyses of the sample at each stage of the study: as-grown, as-treated (HCl and HCl-KCN), and after air aging at an ambient atmosphere (until 120 days). XPS surface chemical analyses are carried out with a Thermo Electron K-Alpha spectrometer using a monochromatic Al-Kα x-ray source (1486.6 eV). The Thermo Electron K-Alpha spectrometer procedure was used to calibrate the spectrometer, and settings are verified using Cu and Au samples following the ASTM-E-902-94 standard procedure.²⁶ Acquisition parameters of high energy resolution photopeaks are 400 μm spot size, 12 kV primary energy, 6.0 mA emission intensity, constant analyser energy mode 50 or 10 eV with 0.1 or 0.05 eV energy step size, respectively. Charge neutralization was not required to perform analyses. Data are processed using the Thermo Fisher scientific Avantage[®] data system. XPS composition is obtained using a Shirley background subtraction and sensitivity factors (SFs) from Avantage[®] library, taking into account of the transmission factor and the inelastic mean-free paths. Photopeaks are fitted using Lorentzian/Gaussian mix. A specific fitting procedure was developed for each photopeak considered (Cu2p_{3/2}, Ga2p_{3/2}, In3d_{5/2}, Se3d,

Ga3d, and In4d), first on reference surfaces, free from oxides and binary compounds, to fix the CIGS matrix parameters. Then, for the as-grown and aged surfaces, additional contributions attributed to oxide and Se side phases (with specific energy positions and FWHM) were added to complete the photopeaks deconvolution. The fitting parameters are presented in Table I.

The CIGS key ratios are quantified using Cu2p_{3/2}, Ga2p_{3/2}, In3d_{5/2}, and Se3d photopeaks. Note that between each XPS analysis, the samples are removed from the XPS holder and so the XPS spot cannot be rigorously positioned at the same locations during the sequential measurements. However, multiple analyses were produced on different random points on the same sample in order to control the distribution and to increase the measurement precision.

III. RESULTS AND DISCUSSION

In the first part of this paper, the chemical evolution induced by two different engineering processes, HCl and HCl-KCN wet treatments, is discussed. Those treatments are performed separately by dipping several pieces of the same as-grown CIGS aged block. The common chemical trends and the slight differences which are pointed out by the comparative approach are discussed.

In the second part, the specific CIGS reactivity under air aging is detailed. This study is performed in the same experimental conditions for HCl or HCl-KCN initially treated surfaces and aims to increase our understanding of the surface chemical evolution after such wet treatments. Compositional values determined on each surface will serve as a baseline to discuss the chemical modifications observed.

In the third part, the case of freshly treated samples (HCl and HCl-KCN) stored under UHV, in the XPS spectrometer chamber, for an equivalent time as the air aging ones is presented. This experience is realized to track an eventual surface chemical evolution under UHV and serves as an element of comparison to precisely determine the origin of the chemical evolution of the fresh etched surfaces.

TABLE I. Summary of the fit results (binding energy—BE, intensity, full width at half maximum—FWHM, concentration) of the Se3d_{5/2} contributions over time for two different chemical treatments.

Aging time	Se 3d _{5/2} contribution	HCl				HCl-KCN			
		BE (eV)	Intensity (counts s ⁻¹)	FWHM	Conc. (at. %)	BE (eV)	Intensity (counts s ⁻¹)	FWHM	Conc. (at. %)
0	CIGS	54.2	1675	0.77	85.5	54.2	1768	0.75	100.0
	Se ⁰	54.7	283	0.77	14.5	—	—	—	0.0
	Oxidized	—	—	—	0.0	—	—	—	0.0
1	CIGS	54.2	1490	0.81	86.1	54.2	1493	0.78	91.8
	Se ⁰	54.6	217	0.81	12.5	54.6	107	0.78	6.6
	Oxidized	58.9	20	0.98	1.4	59.0	19	1.12	1.7
4	CIGS	54.2	1300	0.82	83.3	54.2	1248	0.79	85.5
	Se ⁰	54.8	158	0.82	10.1	54.9	119	0.79	8.2
	Oxidized	58.9	85	0.98	6.6	59.0	80	1.13	6.3
120	CIGS	54.2	722	0.84	60.3	54.2	800	0.82	67
	Se ⁰	54.9	136	0.84	11.4	54.9	134	0.82	11.2
	Oxidized	58.9	242	1.17	28.4	58.9	187	1.15	21.9

A. Chemical modification of the as-grown CIGS surface

All aged as-grown CIGS samples present very close and complex XPS fingerprints (presented in Fig. 1). This is a reproducibility sign of similar aging conditions, from a chemical point of view for all initial surfaces, before HCl or HCl-KCN treatments.

The HCl as the HCl-KCN chemical treatments performed on as-grown samples generate important chemical modifications. In both cases, significant evolutions of the XPS intensities and/or energy distributions are observed, leading to a modification of the inferred compositions. In Fig. 1, such evolutions are presented for the aged as-grown (black bottom spectra) HCl (red mid spectra) and HCl-KCN treatments (blue top spectra), focusing on the Ga3d-In4d, Se3d, Cu3p, O1s, Cu2p, and Na1s/Auger In-MNN regions which give a complete overview of the respective evolutions of the binding energy (BE) distributions and/or the intensities.

The HCl and HCl-KCN treatments display very similar XPS global signatures. Comparing the respective evolutions

of each peak, we note rather analogous trends associated with efficient deoxidation processes. Whatever the chemical soaking the Cu, In, Ga, and Se spectra show comparable global intensities evolutions (and peaks area). They present also similar evolutions of their energy distributions excepted for the Se3d signal. After the HCl treatment, the Se3d peak shape slightly differs from one sample to another and in different positions on a sample. This specificity is illustrated in Fig. 1(c), presenting the extreme variations encountered. Though, this variability is not observed when the following KCN treatment is performed. Note that one of the two spectra observed after the HCl treatment [Fig. 1(c), orange mid-spectrum in a continuous line] shows an energy distribution close to the one observed after additional KCN treatment, but without reaching the ultimate spin-orbit resolution.

Concerning the intensity variations before and after both treatments, a main common observation concerns the opposite trends of O and Cu signals. The decays of the O1s photopeak intensities [Fig. 1(d)] point out an efficient and equivalent deoxidation, leading to a weak signal close to

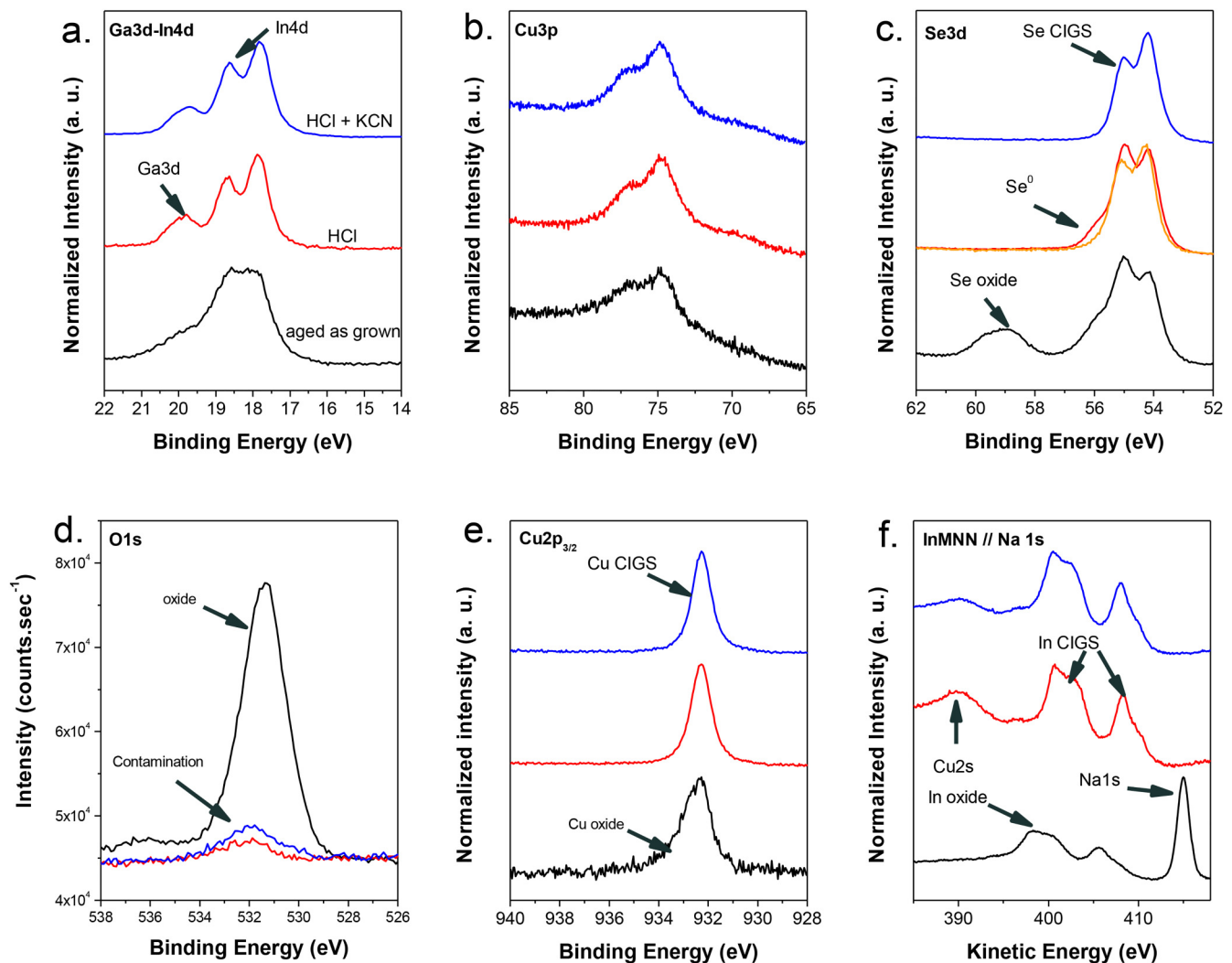


Fig. 1. High energy resolution XPS photopeaks measured on as-grown CIGS (black bottom spectra), after HCl treatment (red mid spectra) and after HCl-KCN treatment (blue top spectra): (a) Ga3d-In4d, (b) Cu3p, (c) Se3d, (d) O1s, (e) Cu2p, and (f) Na1s//Auger In-MNN regions. Spectra are normalized in the intensity and shifted along the y axis for clarity reason (except for O1s photopeaks).

532.0 ± 0.1 eV (BE), which can be assimilated to the “C–O” bonds associated to a carbon contamination contribution [Fig. 1(d)]. The peak areas of O1s fall by a 10–15 factor with respect to the as-grown initial one. Concerning the atomic overall XPS composition, the contribution of the O element passes from around 50% to 5%–10%. All these observations demonstrate that the oxygenated phases, strongly present at the aged as-grown surface, disappear during the HCl or HCl-KCN treatments. Conversely, the copper peak areas present a significant increase after both treatments. The multiplying factor for the HCl treatment is close to 5 while it is close to 3.5 for the HCl-KCN solutions. Concerning the copper balance, a clear re-emergence of the copper contribution is shown, regardless of the treatment.

Figure 1(a) shows the Ga3d-In4d region, presenting a special interest as it enables the observation of the “column III” element evolutions in the same binding energy domain, and so, for equivalent escape depths. After treatments, similar fingerprints are achieved with the emergence of the In4d spin-orbit feature as well as a better separation between the Ga3d-In4d overlapped peaks. The Ga3d-In4d energy distributions indicate a unique “element III” distribution in the CIGS metallic network. The reproducibility of the relative

energy distribution between the Ga3d and In4d must be pointed out and related to well-defined spin-orbit features.

Last, selenium peak shape is also strongly modified after each treatment. For all samples, the selenium oxide state contribution at BE = 58.9 ± 0.1 eV totally disappears, indicating the complete elimination of the “O–Se” bonds at the CIGS surface. Moreover, as already observed,^{21,23} the main Se3d peak contribution presents, as for the Ga3d-In4d region previously described, an enhancement of the spin-orbit splitting separation. So, in both cases, a clear modification of the energy distributions is observed, associated with the apparition of clean spin-orbit features characteristic of the “level-d”. As said above, the trend is more evident after the HCl-KCN treatment. Furthermore, the In-MNN [Fig. 1(e)] and Ga-LMM (not shown here) Auger lines are also strongly modified, in agreement with a very efficient deoxidation phenomenon.

Figure 2(a) shows the resulting simulation of the Ga3d-In4d region after HCl or HCl-KCN treatments on CIGS samples. In a previous work,²⁷ we demonstrated that, in the absence of oxide phases, the Ga3d and In4d peaks are adequately fitted using only one specific “level-d” contribution for each peak. This simulation enables to determine a

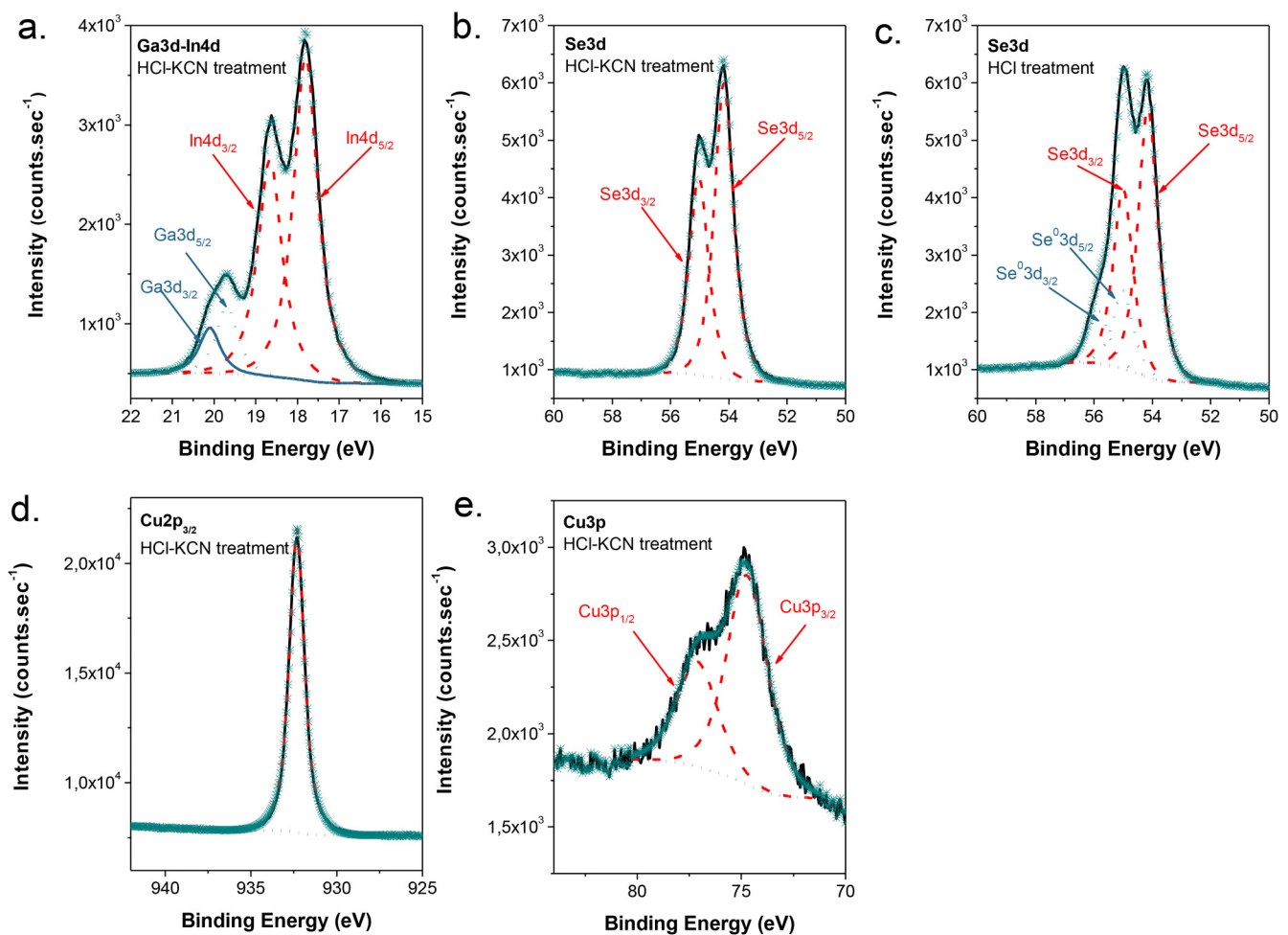


FIG. 2. Peak fitting of (a) Ga3d-In4d, (b) Se3d, (d) Cu2p_{2/3}, and (e) Cu3p regions of an HCl-KCN CIGS treated sample and (c) Se3d core level after HCl treatment.

true GGI value, both In and Ga intensities being attenuated in a similar trend by the superficial carbon contamination layer. A remarkable point is that for HCl and HCl-KCN treatments, we obtained similar fitting parameters in this Ga3d-In4d region. This tends to indicate that, irrespective of the chemical treatment, the same chemical state and composition are reached for Ga and In elements, corresponding to the CIGS lattice response. Identical conclusions are drawn concerning the In3d or Ga2p more commonly used windows.

Figures 2(b) and 2(c) illustrate two fitting configurations of the Se3d region. Contrary to Ga3d-In4d region previously described, the Se3d peak shape differs with the treatment employed. However, for both chemical treatments, a complete elimination of oxidized selenium contribution situated at BE = 59.0 ± 0.1 eV is visible, but also an evolution of the energetic distribution of the global Se3d region from 52 to 57.5 eV. Indeed, a better spin-orbit splitting is obtained^{21,23} as well as a thinning of the apparent global FWHM_{Se3d} (full width at half maximum for the region 52–57.5 eV) from 1.84 (as-grown) to 1.61 (HCl) and 0.95 ± 0.05 eV (HCl-KCN).^{18,23,28,29} Interestingly, this evidences a distinction between HCl [Fig. 2(c)] treated surfaces and the ones treated by HCl-KCN [Figs. 1(c) and 2(b)]. The important difference of FWHM values between HCl and HCl-KCN treatments indicates at least one additional Se environment in the case of HCl process, leading to a fitting procedure with one “3d-level” double contribution for the HCl-KCN treatment, while another double contribution positioned at 54.6–56.5 eV²³ is required to completely simulate the Se3d spectrum for the HCl treatment. Indeed, as expected with the Se potential-pH diagram, the HCl deoxidation process does not eliminate all the Se side species present in the aged as-grown surfaces which, in the CIGS case, can be attributed to Se⁰ or Se binary phases such as Cu_{2-x}Se. In Fig. 2(c), the case of the ultimate deformation of the Se3d signal we observed is presented, giving a ratio Se⁰ – Se_{Cu_{2-x}Se}/Se_{CIGS} of 0.30. Note that this ratio decays close to 0.10 for the lowest deformation. Obviously, after the HCl-KCN treatment, the steadiness of the Se3d peaks energy distributions demonstrates a complete elimination of elementary side Se species contributions and reproducible surface. In the case of HCl, variability is observed [Fig. 1(c), red and orange middle spectra]. Indeed, side phases present at the as-grown surface, such as Se⁰ or Cu_{2-x}Se, are sometimes

totally or partially maintained at the surface during the deoxidation process. Moreover, the variation of the Se3d energy distribution in the 55.0–56.5 eV range observed after the HCl treatment indicates a complex etching process. Considering that the Se3d response of the as-grown aged surface is almost constant on initial samples, the observed fluctuation should then be generated by the chemical oxide elimination step. The initial CIGS surface chemistry is thus very complex and presents a superficial complex mixture of Ga, In, Se oxides phases to which selenium side compounds are also added. The different residual Se⁰ and Cu_{2-x}Se phases' contents at the surface can only be explained if a differential dissolution occurs, the side compounds situated in the external part of the superficial oxidized layer being taken off at the same time as the oxides although the ones directly in contact with the CIGS surface are more stable and maintained. Concerning copper, both Cu2p and Cu3p photopeaks mainly show an increase in their peak intensities but without significant modification of their energy distributions (position and FWHM). The observations are the same for HCl and HCl-KCN treatments [Figs. 1(b) and 1(e)]. The Cu chemical environment can be considered as specific of Cu(I) contribution in agreement with the Cu2p_{3/2} BE at 932.20 ± 0.05 eV³⁰ as well as the Auger parameter. Indeed, Auger parameters of Cu(0) or a Cu(II) are tabulated at 1851.3 and 1851.8 eV, respectively,³⁰ and the present CIGS Auger parameter calculated is 1849.3 eV. This value comforts a Cu(I) oxidation state, whose corresponding Auger parameter is in a range of 1848.7–1849.7 eV.³⁰ Cu2p or Cu3p levels are well fitted with only one contribution whose doublet positions are fixed by the spin-orbit coupling [Figs. 2(d) and 2(e)]. For the as-grown sample, we have a superficial Cu-poor overlayer at the surface constituted of Cu in the CIGS matrix only or a copper-selenide matrix, without apparent Cu oxide phases. The main observation in this paper is that the relative Cu intensity increase is more important after the HCl treatment than after HCl-KCN one, leading to a higher apparent global CGI ratio (Table II), as it will be discussed below. Qualitatively it can be related to the presence of the additional Se species in the Se3d window. As described above for HCl, additional Se contribution can be assigned to the presence of a Cu_{2-x}Se binary phase or elementary Se⁰ phase on the deoxidized CIGS surface. Note that this feature is concomitant with the Ga, In, and Se oxide species elimination.

TABLE II. Evolution of the overall XPS key ratios: GGI = [Ga]/([Ga] + [In]), CGI = [Cu]/([Ga] + [In]), and 2 * VI/(I + 3 * III) = (2 * [Se])/([Cu] + 3 * ([In] + [Ga])) measured on as-grown CIGS, after HCl or HCl-KCN treatment and after air reaging (until 120 days). The standard error bar for each ratio is evaluated at ±0.05. Cu2p_{3/2}, Ga2p_{3/2}, In3d_{5/2}, and Se3d photopeaks are used for quantification.

	HCl			HCl-KCN		
	GGI	CGI	2 * VI/(I + 3 * III)	GGI	CGI	2 * VI/(I + 3 * III)
As-grown	0.26	0.19	1.07	0.26	0.19	1.07
t ₀	0.37	1.09	1.52	0.35	0.69	1.23
1 day air aging	0.37	0.96	1.39	0.35	0.59	1.18
4 days air aging	0.36	0.70	1.34	0.35	0.46	1.05
120 days air aging	0.32	0.52	1.39	0.33	0.36	1.03

The last main feature related to both treatments is the total disappearance of the Na1s contribution [Fig. 1(e)]. This means that the Na signal, which is clearly detected on as-grown aged surfaces, is totally removed from the CIGS surface using the two aqueous treatments. The chemical environment of Na1s (1071.6 ± 0.1 eV in BE) is not yet fully understood due to photopeaks with large FWHMs on the initial aged surfaces but Calvet *et al.*³¹ suggest some specific chemical environments with Na₂SeO₃ species especially.

Using peak simulations, presented in Fig. 2, we conclude that, starting from a strongly oxidized as-grown surface, reproducible free oxide CIGS surfaces are easily obtained with HCl or HCl-KCN treatments. However, the HCl-KCN provides a more efficient cleaning procedure as eventual side selenide phases are also eliminated. Therefore, both treatments provide chemical states close to a pure CIGS reference surface. In particular, for the HCl-KCN one, all the signals emitted by the Cu, In, Ga, and Se atoms only come from the CIGS layer lattice. Consequently, the atomic compositions deduced from the different photopeaks intensities correspond to a well-defined CIGS surface and the associated values can be considered as a reference set of data.

In term of quantitative analysis, the intensities associated with the Cu2p, In3d, Ga2p, and Se3d are used to provide the XPS compositions of the treated surfaces without any simulation. We chose this set of peaks because they are the classical levels used in the literature, more intense and not perturbed by any overlapping. The deduced GGI, CGI, and $2 * VI / (I + 3 * III)$ representative ratios determined with this set of peaks are given in Table II. As published recently,^{27,32,33} the fitting of the Ga3d-In4d window [Fig. 2(a)] also enables to determine the GGI value on the reference treated surfaces. Using these data, the GGI is close to 0.30. However, we did not use this window for the global quantification evolution, as this simulation is only reliable for an oxide-free reference surface and becomes more ambiguous and source of error as soon as Ga or In oxide phases must be considered.

The XPS compositional values given in Table II for the fresh treated samples agree with the discussion on the common and different points deduced from the peak simulations in Fig. 2. Analysis of the GGI values shows that they are equal after HCl or HCl-KCN treatments. This uniqueness corresponds to the fact that all the Ga or In regions present similar deconvolutions between the different chemical treatments. Fig. 2(a) associated with the simulation of the Ga3d-In4d window emphasizes this point. The CGI values differ significantly after HCl or HCl-KCN treatments (1.09 ± 0.05 and 0.69 ± 0.05 eV). This, on one hand, agrees with the fact that the resurgence of the copper signal is stronger for the HCl treatment and on the other hand with the fact that Se3d signals are different after HCl treatment, with a need to introduce the second component in the simulation. Therefore, the copper signal for the HCl-KCN treatment can be attributed to the lone contribution of CIGS lattice, while for the HCl treatment, a supplementary contribution, attributed to Cu_{2-x}Se side phase or even to Se⁰ one, must be considered. As these side phases do not provide chemical displacement toward the Cu contribution in CIGS, it is

impossible to distinguish between the two on the basis of the spectrum simulation alone. Only the quantitative approach present in the CGI value difference contains the information. Finally, the CGI value measured by XPS on the clean CIGS surface is close to 0.7. This low value will be commented below.

B. Evolution of the treated CIGS surfaces under air aging

Starting from the fresh initial HCl or HCl-KCN cleaned surfaces, the evolution toward a reoxidation process under air interaction is studied. The knowledge of the reoxidation mechanism must bring important information about the chemical trends of the CIGS surfaces when exposed to air. Moreover, with initial surfaces with or without side Se signal, such investigation can also shed light on the extent of the influence of partial (or not) coverage of the surface by Se side phases.

Cleaned surfaces, aged without air exposure, will be used as an essential element of comparison. This can be achieved by keeping the treated samples in either a neutral atmosphere, such as nitrogen or argon environment, or under vacuum. For this work, we chose the UHV environment, with storage times equivalent to the longer ones used for air exposure.

The key result in the UHV environment is that the CIGS surface states obtained after HCl or HCl-KCN treatments are stable over 120 days (Fig. 3), without observable chemical modifications of the XPS spectra nor compositional ratios evolution. Such stability indicates that no spontaneous evolution of the surface due to surface instability occurs, and so no atomic reorganization related to intrinsic surface lattice instability of the quaternary alloy. This result is the same in the presence or not of side Se phases (for HCl). Therefore, all the interactions observed for surfaces exposed to air must be linked to their specific reactivity toward this environment.

Each sample was aged under the same ambient air condition. Their chemical evolutions were controlled by XPS characterizations at different stages: 1, 4, and 120 days. Even during aging, after HCl or HCl-KCN treatments, similar evolutions of the high energy resolution XPS spectra are observed, despite the slightly different starting states. The obtained spectra are shown in Figs. 4 and 5 using the Cu2p_{3/2}, Ga2p_{3/2}, In3d_{5/2}, Ga3d-In4d, Se3d, and O1s peak regions for HCl and HCl-KCN chemical treatments, respectively. In opposition to the complete stability under UHV (Fig. 3), the reoxidation process observed under atmosphere puts forward a progressing mechanism of the reactive reorganization of the outer layer. The main features can be summarized through an expected increase of the oxygen peak intensity [Figs. 4(f) and 5(f)] and a decay of the copper one compared to In and Ga signal evolution. Concerning the shape of the peaks, the global trend observed for each element is to develop new contribution associated with the apparition of oxygen bonds with Ga, In, Se, and, at a longer timescale, with Cu. Therefore, after 4 months at air exposure, a stabilization of the

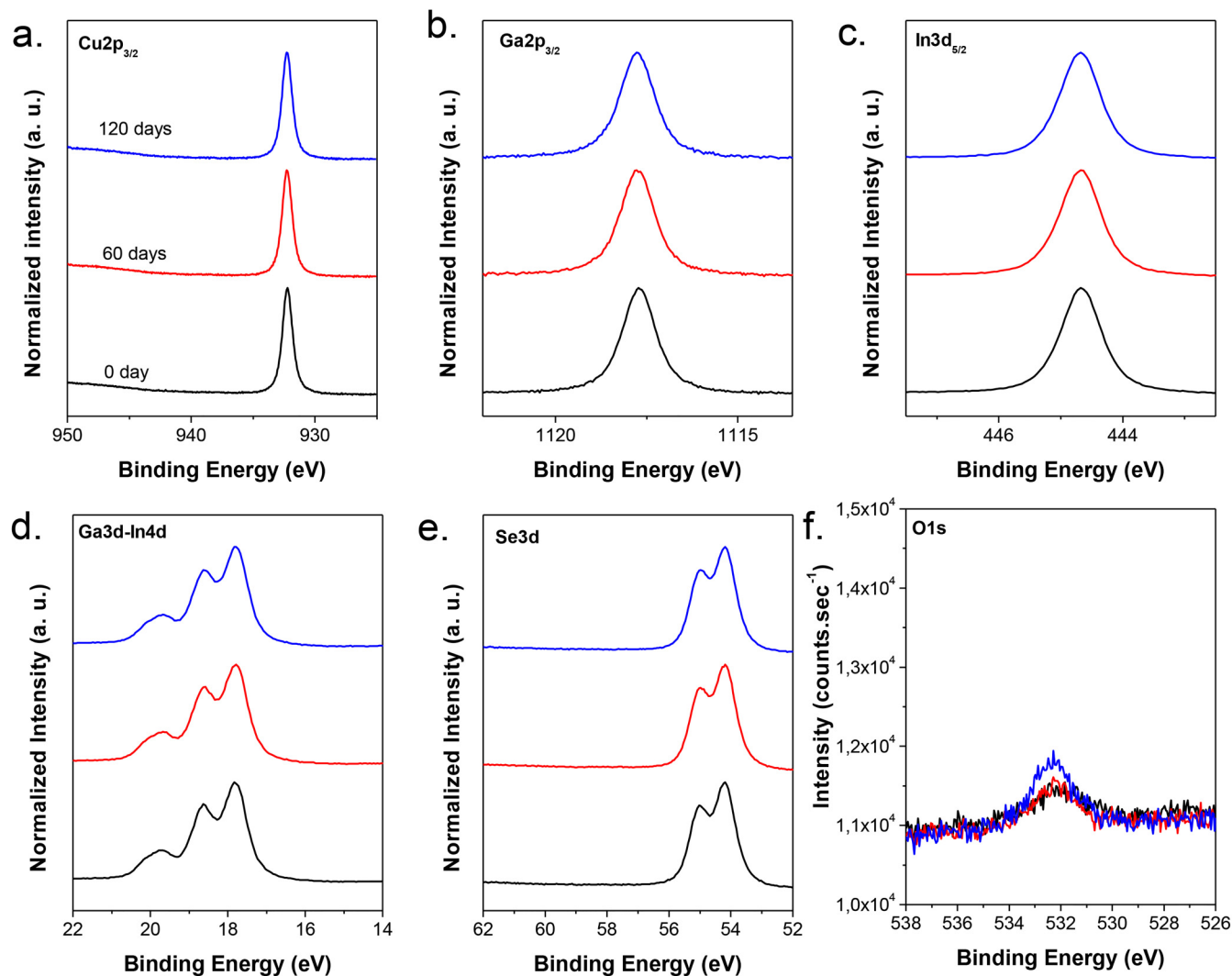


Fig. 3. Evolution over time of high energy resolution XPS photopeaks of CIGS after HCl-KCN treatment under UHV conditions: (a) Cu_{2p_{3/2}}, (b) Ga_{2p_{3/2}}, (c) In_{3d_{5/2}}, (d) Ga_{3d}-In_{4d}, (e) Se_{3d}, and (f) O_{1s} regions. Spectra are normalized and shifted along the y axis for clarity reason (except for O_{1s} photopeaks).

surface chemical modification seems to be reached. For HCl and HCl-KCN treatments, the reoxidation process leads to the very similar oxidized surface but this final state is nevertheless slightly different, even though close to the aged as-grown one, more oxidized.

Concerning the evolution of the III's element, the modification of the Ga_{3d}-In_{4d} [Figs. 4(d) and 5(d)] spectral distribution directly brings a comparative evolution. Indeed, a less defined spin-orbit is noticed, attributable to the narrowness of the BE distribution of In_{4d}. Moreover, a less visible separation between the 3d and 4d levels due to a partial overlapping between the Ga and In peaks which progresses in time. Both modifications are attributed to the emergence of Ga-O and In-O chemical bonds. Similar broadening effects are observed for the Ga_{2p} [Figs. 4(b) and 5(b)] or In_{3d} [Figs. 4(c) and 5(c)] windows as well as modifications of the In-MNN and Ga-LMM Auger lines (not shown here), presenting similar fingerprints as the one of the as-grown aged sample. As previously mentioned, a complex fitting procedure of the Ga_{3d}-In_{4d} window has to be performed in the presence of oxides, and in this paper,

conventional Ga_{2p} and In_{3d} regions are preferred to provide compositional information evolutions.

Concerning the progression of the oxidation process, the evolution of the Se window [Figs. 4(e) and 5(e)] is the richest in term of information. As for the Ga_{3d}-In_{4d} window, but over a larger energy distribution, the continuous modification is also evidenced with a characteristic deformation of the low binding energy region in the 55–56.5 eV range. Progressively again, less defined spin-orbit features are shown because of the Se⁰ contribution formation and increase (HCl and HCl-KCN). This is accompanied by the re-emergence of the high binding energy contribution close to 58.9 eV, related to the appearance of the Se-O bonds.

Finally, for both initial treated surfaces, the spectral evolutions tend to the as-grown distribution even if the deformations are less important.

This double evolution of the Se region is very interesting to discuss. Analysis of the short time evolution of the Se_{3d} region shows that Se⁰ contribution appears earlier than the oxide one (Table I and Fig. 6). This is an established trend, even if quantitative time considerations are difficult to propose

HCl treatment

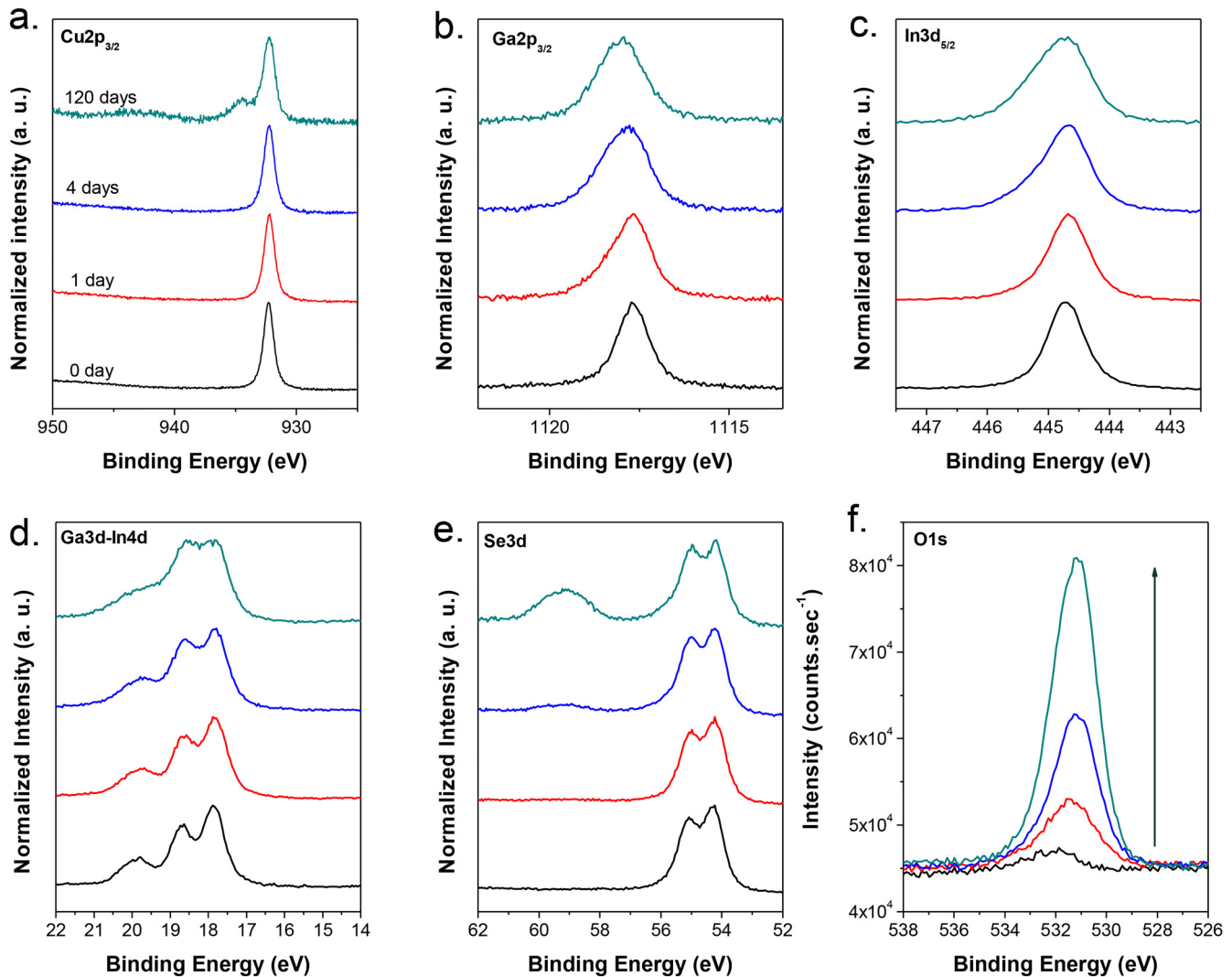


Fig. 4. Evolution over time of high energy resolution XPS photopeaks of CIGS after HCl treatment: (a) Cu2p_{3/2}, (b) Ga2p_{3/2}, (c) In3d_{5/2}, (d) Ga3d-In4d, (e) Se3d, and (f) O1s regions. Spectra are normalized and shifted along the y axis for clarity reason (except for O1s photopeaks).

at this time. This delay suggests that a direct Se–O bond creation is rather improbable and a complex oxidation mechanism for which oxidation intermediates as Se⁰ species are involved is more likely to occur. This is a classical feature when we consider the anodic oxidation process of II–VI compounds for which VI⁰ (Se or Te) species are clearly established as corrosion intermediates.^{34,35} It is worth noting that the evolution of the Se signal is obviously not related to Cu one as the Cu content decreases. Therefore, new Cu-selenide phases that could provide the same intermediate binding energy features must be excluded.

The small FWHM time evolutions observed in Table I (from 0.77 to 0.84 eV for HCl and 0.75 to 0.82 eV for HCl + KCN chemical treatments) could be possibly due to a differential charging effect but also to a local fluctuation of the surface potential as the material is polycrystalline.

Concerning the copper [Figs. 4(a) and 5(a)], the main feature is its strong signal decrease compared to Ga, In, and

Se ones. This specific decay implies a new copper-poor surface formation as the lone consequence of the oxidation process. The interest of these aging experiments is that the decay is perfectly controlled. Moreover, long time air aging can sometimes lead to a new weak contribution on the Cu2p photopeak, at higher BE = 934.50 ± 0.05 eV, which can be assimilated to CuO presence. Such small side Cu2p contribution is more or less marked according to the starting chemical treatment and to the sample. In both cases, starting from well-known initial surfaces, the controlled aging sequences point out a gradual loss of Cu established by the CGI decrease which tends to the value measured on the as-grown aged surface. Thus, this paper obviously demonstrates that the Cu losses are related to the oxidation process on CIGS surfaces and its surface chemical reorganization.

Finally, the last important observation is the re-emergence in time of the Na1s contribution which starts to be visible from the second day at air exposure. Starting both treatments

HCl-KCN treatment

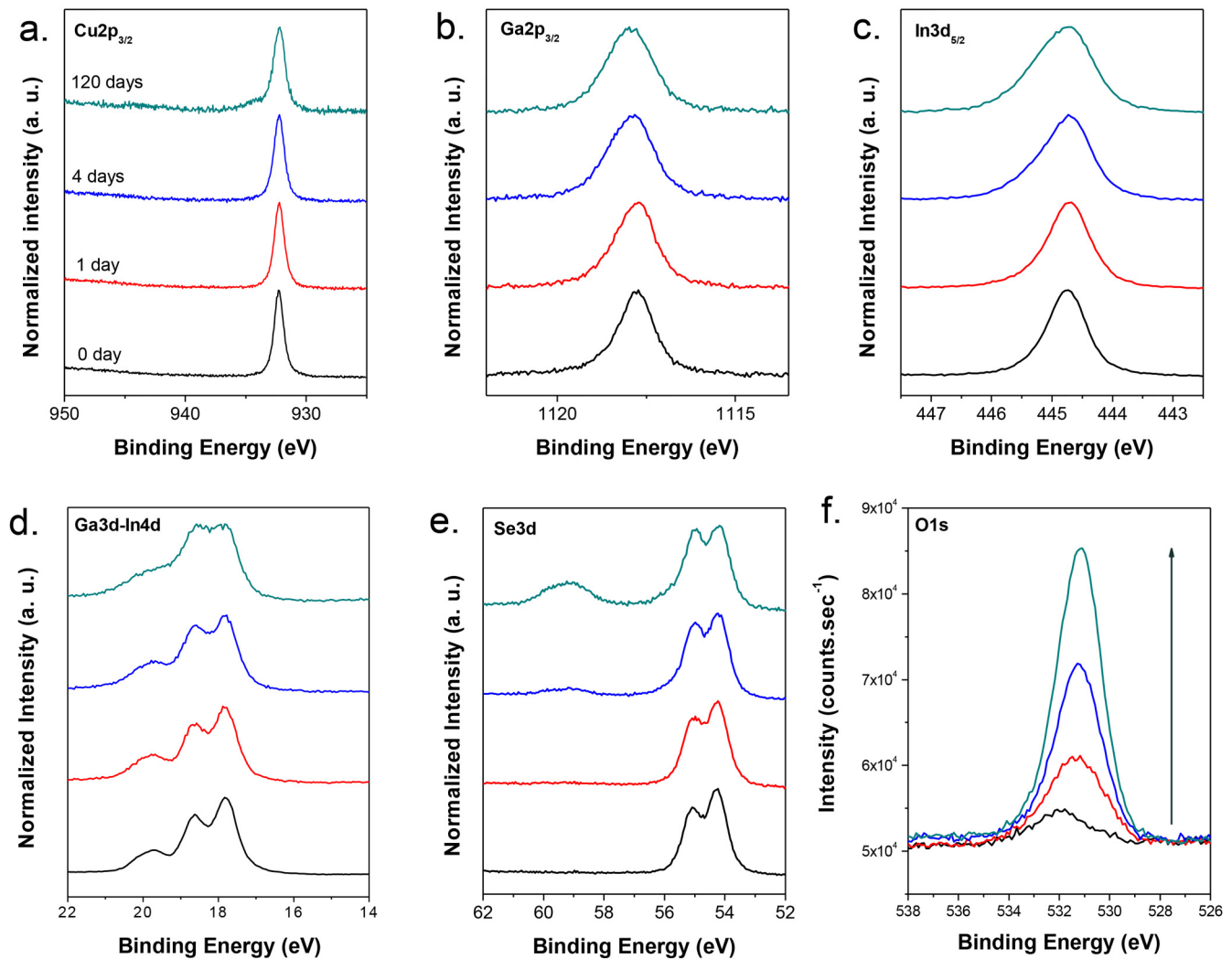


FIG. 5. Evolution over time of high energy resolution XPS photopeaks of CIGS after HCl-KCN treatment: (a) Cu_{2p_{3/2}}, (b) Ga_{2p_{3/2}}, (c) In_{3d_{5/2}}, (d) Ga_{3d}-In_{4d}, (e) Se_{3d}, and (f) O_{1s} regions. Spectra are normalized and shifted along the y axis for clarity reason (except for O_{1s} photopeaks).

with Na free surface, this reappearance during the reoxidation process is linked to an outward migration through the CIGS layer of Na incorporated inside the CIGS bulk and from the soda-lime glass deeper. However, the Na amount detected by XPS is lower by a factor 30–50 than the one reached on aged as-grown surfaces. The absence of Na on treated sample surfaces maintained under UHV storage evidences a direct relation of Na migration with the reoxidation process.³⁶ This result is an important experimental observation, proving that under UHV, the Na migration is no longer active, at least at the time scale chosen here (120 days).

Cu, Ga, In, and Se spectra distributions were found to present similar evolutions, pointing out the significance of the quantification shown in Table II. This table provides the global values of the GGI, CGI, and $2 * VI / (I + 3 * III)$ specific ratios at the different stages of the CIGS surface evolution, in the so-called homogeneous model approximation³⁷ which brings an overall composition of the CIGS matrix and the oxide and side Se phases outer layer stacking of

aged surfaces (as-grown and reaged). To separate the outer layer contribution from the matrix one beyond, spectra deconvolution is required (Fig. 6). An accurate fitting procedure has been developed, starting from the simulation of spectra obtained on bare CIGS to determine the CIGS material fitting parameters and then implemented on the aged surfaces with additional contributions corresponding to the external region contribution containing compounds issued from the surface reactivity.

Looking at the global compositional ratios, similarities and variations between the treatments must be pointed out. After 120 days aging, the GGI ratios remain almost constant, without significant differences observed depending on the applied chemical treatment. This observation is independent of the Ga and In elements' environments (oxide and CIGS matrix), the global quantity remains almost constant, with a GGI around 0.34 ± 0.05 , for the samples used in this paper.

Concerning the copper balance, the starting points are different but a common trend is observed through a global

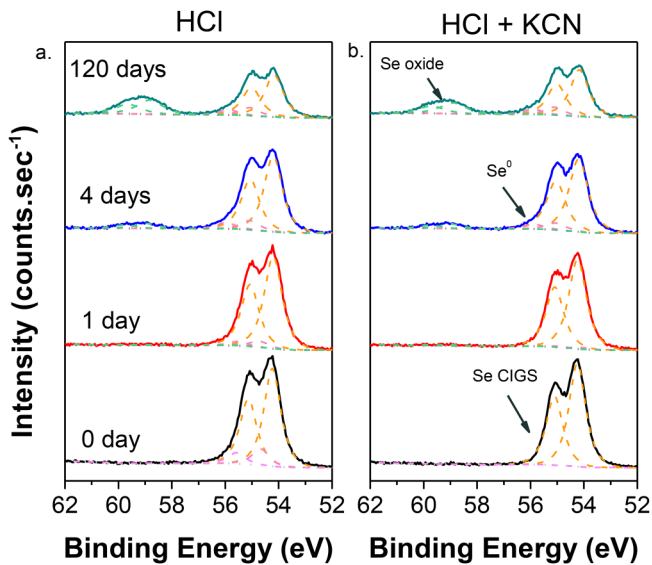


Fig. 6. Evolution over time of high energy resolution Se3d regions with the deconvolution XPS photopeaks of CIGS after HCl (a) and HCl-KCN treatment (b).

decrease of the CGI ratios after both treatments. After the HCl treatment, the air exposure leads to the CGI decrease, from 1.09 ± 0.05 to 0.52 ± 0.05 , whereas after the HCl-KCN treatment, the CGI changes from 0.69 ± 0.03 to 0.36 ± 0.05 . It is obvious that the HCl treated surfaces keep their initial Cu-rich composition after air aging, despite their progressive apparent copper loss. As it was previously presented in Fig. 2(c), this is due to the presence of Cu_{2-x}Se binary phase at the CIGS surface after the HCl treatment. Compared to HCl-KCN, this copper enrichment is not eliminated with air aging and the oxidation process gives rise to the preservation of the initial surface chemical configuration. It is noteworthy that this specific phase can be modulated with long time immersions in HCl or a careful rinsing phase, with always a decay but never its complete elimination. This suggests that the side copper-selenide phase is also involved in the aging process independently from the CIGS one. The slight copper oxide phase detected sometimes could be related to this partial oxidation of the side phase, but not only, because similar features are also detected on HCl-KCN treated surfaces after a long time aging. The HCl-KCN process leads to the same decay behavior in time but with a smaller CGI variation range after the chemical treatment. So, this final CGI value and its evolution under air aging must be considered as representative of the specific Cu decay observed on a clean reference CIGS surface free from the side phases. This affirmation is supported by the discussion on the peak fitting procedure performed in Fig. 2, which agrees with an uncovered CIGS reference surface, without oxides and Se side phase.

All these Cu, In, and Ga information need to be associated with the Se quantity variations at the surface. We chose the ratio $2 * VI / (I + 3 * III)$ representative of the charge balance of the quaternary alloy.³⁸ As for GGI and CGI, the ratio is obtained using the total Se element contribution,

i.e., without fitting consideration on Se-O, Se⁰, and Cu_{2-x}Se possible additional contributions to the CIGS one. Indeed, the difficulty in the Se3d main peak quantification is to discriminate the contribution linked to a Cu_{2-x}Se binary phase and an elementary Se⁰.²³ Consequently, in Table II, we only focus on the $2 * VI / (I + 3 * III)$ global ratio covering all the Se chemical states and their relevant contributions which provide global compositional trend between the Se and the metallic elements. The HCl-KCN and the HCl treatments lead to different values close to $1.23 (\pm 0.05)$ and to $1.52 (\pm 0.05)$, respectively. The XPS deviation from the expected value of 1.00³⁸ is discussed in the following part. Once again, the surfaces freshly treated by HCl-KCN present significant lower values in relation to the observed Cu concentration. For both deoxidized surfaces, we observe a global decay in relation with the air exposure, with the ratios falling to $1.39 (\pm 0.05)$ for HCl treated surfaces and to $1.03 (\pm 0.05)$ for the HCl-KCN ones. Such evolution means that the Se balance is strongly modified by the reoxidation process induced by air aging, with an apparent loss of this element. This evolution is concomitant with the qualitative observations as Ga and In reoxidation processes occur prior to Se and Cu ones. So, the quantitative balance of Se at the surface is strongly modified with an apparent loss which, as for the Cu, requires an explanation.

Concerning the initial difference between surfaces treated with HCl and HCl-KCN, the higher $2 * VI / (I + 3 * III)$ ratio is consistent with the fact that the HCl treatment does not eliminate the side Se phase. Such results can be linked to the CGI ratio increase and thus partly attributed to the formation of a Cu_{2-x}Se binary phase and Se⁰ one. Despite being qualitatively coherent, several questions arise from the reported absolute values. For a fresh HCl-KCN surface, all the information given by the high energy resolution peaks fitting agree with very clean surfaces without surface oxide or side selenide phases covering, implying that only the CIGS atomic lattice is probed by XPS. However, as mentioned above, the values in the range 1.3–1.4 markedly differ from the 1.0 expected.³⁸ We have noted that this ratio is very stable even in the case of a long time UHV storage, indicating a perfect stability of the lattice sheltered from air exposure. Such a ratio is a well-established XPS information for clean surfaces and would mean that, near the surface of the CIGS samples, Se rich phases would exist even after the KCN treatment. This is very difficult to reconcile with the high solubility rates of all these phases via the KCN etching. Moreover, this assumption about residues of side Se phases can be totally excluded considering the Se3d peak fitting. This composition deviation is then more probably explained by the composition calculation itself.

One parameter which can explain the observation of the apparent overestimation of the Se percentage is the differential screening of all the photopeak intensities by the adventitious carbon contamination^{27,31} which is always present on the CIGS surfaces after aqueous chemical treatments, as after their following air transfer toward UHV. The screening of the actual CIGS signal by the contamination layer perturbs the estimation of the authentic atomic composition of the surface.

As previously discussed for the GGI determination,²⁷ in the case of the CIGS, it is particularly true because the kinetic energies of the photoelectrons emitted by the used Ga2p, Cu2p, In3d, and Se3d core levels are very different, so this large distribution implies that the intensity attenuation by the carbon overlayer differs for all those peaks. In addition, due to the fact that the exact C1s peak totally overlaps with the Se-L₃M₂₃M₄₅ Auger line, an accurate estimation of the carbon content is not obvious. Thus, one plausible explanation for the high value of the $2 * VI / (I + 3 * III)$ ratio could be the lowest screening of the Se3d contribution due to its very high kinetic energy (~1432 eV) and so the deeper origin of photoelectrons.³⁷ The $2 * VI / (I + 3 * III)$ XPS ratio comprised in a 1.3–1.4 range can be considered as characteristic of the clean CIGS surface but obviously overestimated.

A second possible origin for the XPS overestimation of the Se balance can be the value used for the SF associated with the Se3d core level. Using the AI THERMO SF[®] database, the proposed SF for the Se3d is a value of 1.6 which strongly differs from the 2.29 value proposed in the conventional Scofield table. So, the exact value of the SF Se3d remains an open question out of the topic of this paper and which would need the assistance of references analysis on samples such as CdSe or ZnSe. Definitely, a modification of the SF Se3d value from the tabulated one (1.6) to 2.3 induces a variation of the $2 * VI / (I + 3 * III)$ ratio from 1.23 to 0.56 for the HCl-KCN reference sample. Nevertheless, the comparative data provided in this paper are sufficient and coherent to describe the evolution of the Se balance induced by the air reactivity onto CIGS surfaces.

Thanks to the fine study of the ratios evolution during the reoxidation of bare CIGS surfaces, we have gained a strong knowledge concerning the reorganization of the CIGS surface during the oxidation process at air exposure. Global consideration based on our results establishes a multistep process occurring at the surface. (i) The oxidation of a clean initial CIGS surfaces, with or without residual selenide side phase, gives rise to a very complex outer layer formation with an important redistribution of the constituting elements and continuous incorporation of oxygen. The new elements brought by our study are that the reoxidation processes reported here start from well-defined and cleaned surfaces. (ii) Obviously, there is also a significant superficial copper loss whose origin must be considered seriously, as the global Se amount also decreases in relation with the strong oxygen enrichment directly correlated to the formation of Ga and In oxygen bonds. (iii) Se atoms are found to form also Se–O surface bonds in time. The balance between the oxygen gain and the Se loss is an unresolved question as well as the very strong Cu loss, in quantitative terms. The Se signal at low binding energy also changes strongly, indicating that oxidation induces the apparition of an Se⁰ phase. Its initial appearance during the first air aging steps suggests that Se⁰ must be considered as an oxidation intermediate and a parallel can be drawn with anodic oxidation on II–VI compounds.^{34,35} (iv). During reoxidation in ambient conditions, a concomitant Na migration toward the surface, possibly through the grain boundaries, is also evidenced, which is not observed during UHV aging.

IV. SUMMARY AND CONCLUSIONS

In this paper, wet chemical treatments are performed on aged as-grown CIGS samples to provide initial reproducible clean CIGS surfaces (oxide and Se side compounds elimination). The novelty of the present work relies on the fine analysis of the reoxidation process performed on the previously cleaned surface. This approach allows a better understanding of the oxidation process and of CIGS surface reactivity toward air and UHV. The treatments evaluated in this work are HCl soaking and HCl-KCN sequential immersions which provide a similar surface composition characteristic of a very efficient deoxidation effect. However, the HCl treatment leads to a different CIGS surface, Cu-rich, and presenting residual Se side phase, whose distribution appears variable from a sample to another and at different localizations on the same sample. The oxidized phase is well removed by all treatments but the Cu_{2-x}Se binary phase is only removed by the KCN wet process leading to remarkable reproducible and well-defined CIGS representative surfaces.

In both cases, the reoxidation process is quite similar and appears to be really slow, as it can only be clearly observed after 4 days at air exposure. For HCl-KCN treated surfaces, oxidation starts with the reappearance of Se⁰ prior to oxide formation, acting as a corrosion intermediate. Then, initially, “In–O” and “Ga–O” bonds are formed, followed by “Se–O” ones leading to an overlayer constituted of In, Ga, and Se complex oxide mixture and so again a Cu-poor surface. Cu oxide becomes visible at larger timescales. Nevertheless, the depletion never reaches the value measured on the as-grown aged samples for the aging duration studied (until 120 days).

Na is completely removed from the CIGS surface by both chemical treatments. It always reappears in time at the surface, due to the soda-lime glass unlimited reservoir at the back contact. Na migration is concomitant with the oxidation process and does not re-emerge on the surface under UHV conditions.

This paper gives a detailed approach of the CIGS surface reactivity in interaction with the ambient atmosphere and proposes an initial global model of oxidation process steps occurring at air. Note that the perfect stability of the surface under UHV storage emphasizes that the origin of the very strong atomic rearrangement is only due to the oxidation mechanism and not to intrinsic material instabilities. This study also shows how a pristine surface can be regenerated. Both processes are extremely relevant for technological applications involving CIGS material. In addition, the present work asks important questions which still need to be explored, such as where does the copper go during the reoxidation process? What are exactly the phases at the CIGS surface and in which proportion? How does the sodium move through the different layers? Did it diffuse through grain boundaries? To answer these questions, a specific study is already underway on a batch of flattened CIGS samples analyzed by XPS and angle resolved XPS.

ACKNOWLEDGMENTS

The authors thank Wolfram Hempel from ZSW, Germany and Sofia Gaiaschi and Patrick Chapon from Horiba Scientific

for CIGS samples supply. This work has been carried out in the framework of the project I of IPVF (Institut Photovoltaïque d'Ile-de-France). This project has been supported by the French Government in the frame of the program "Programme d'Investissement d'Avenir—ANR-IEED-002-01."

- ¹J. H. Werner, J. Mattheis, and U. Rau, *Thin Solid Films* **480–481**, 399 (2005).
- ²T. Kato, *Jpn. J. Appl. Phys.* **56**, 04CA02 (2017).
- ³M. Powalla, S. Paetel, E. Ahlswede, R. Wuerz, C. D. Wessendorf, and T. Magorian Friedlmeier, *Appl. Phys. Rev.* **5**, 041602 (2018).
- ⁴J. Wu, Y. Hirai, T. Kato, H. Sugimoto, and V. Bermudez, *7th World Conference on Photovoltaic Energy Conversion (WCPEC-7)*, Waikola, HI, 10–15 June 2018 (IEEE, New York, 2018), p. 10.
- ⁵H. Sugimoto, *40th IEEE Photovoltaic Specialists Conference*, Denver, CO, 8–13 June 2014 (IEEE, New York, 2014).
- ⁶M. A. Green, Y. Hishikawa, E. D. Dunlop, D. H. Levi, J. Hohl-Ebinger, M. Yoshita, and A. W. Y. Ho-Baillie, *Prog. Photovoltaics Res. Appl.* **27**, 3 (2019).
- ⁷N. Naghavi et al., *Prog. Photovoltaics Res. Appl.* **18**, 411 (2010).
- ⁸S. Niki, M. Contreras, I. Repins, M. Powalla, K. Kushiya, S. Ishizuka, and K. Matsubara, *Prog. Photovoltaics Res. Appl.* **18**, 453 (2010).
- ⁹C. J. Hibberd, E. Chassaing, W. Liu, D. B. Mitzi, D. Lincot, and A. N. Tiwari, *Prog. Photovoltaics Res. Appl.* **18**, 434 (2010).
- ¹⁰A. Chirilă et al., *Nat. Mater.* **10**, 857 (2011).
- ¹¹M. Powalla, S. Paetel, D. Hariskos, R. Wuerz, F. Kessler, P. Lechner, W. Wischmann, and T. M. Friedlmeier, *Engineering* **3**, 445 (2017).
- ¹²S. B. Zhang, S.-H. Wei, A. Zunger, and H. Katayama-Yoshida, *Phys. Rev. B* **57**, 9642 (1998).
- ¹³J.-F. Guillemoles, L. Kronik, D. Cahen, U. Rau, A. Jasenek, and H.-W. Schock, *J. Phys. Chem. B* **104**, 4849 (2000).
- ¹⁴S. Pecharmant, J. Guillemoles, J. Vedel, D. Lincot, J. M. Siffre, H. Ardelean, and M. Marcus, *Proceedings of the 11th International Conference on Ternary and Multinary Compounds, ICTMC-11*, Salford, 8–12 September 1997 (Inst. of Physics Publ., Bristol, 1998), p. 719.
- ¹⁵J. F. Guillemoles, *Thin Solid Films* **403**, 405 (2002).
- ¹⁶P. K. Johnson, A. O. Pudov, J. R. Sites, K. Ramanathan, F. S. Hasoon, and D. E. Tarrant, *Proceedings of the 29th IEEE Photovoltaic Specialists Conference*, New Orleans, LA, 19–24 May 2002 (IEEE, New York, 2002), pp. 764–767.
- ¹⁷K. Ramanathan, F. S. Hasoon, P. K. Johns, and J. R. Sites, *J. Phys. Chem. Solids* **64**, 1495 (2003).
- ¹⁸B. Canava, J. F. Guillemoles, J. Vigneron, D. Lincot, and A. Etcheberry, *J. Phys. Chem. Solids* **64**, 1791 (2003).
- ¹⁹B. Canava et al., *Thin Solid Films* **431–432**, 289 (2003).
- ²⁰J. Kessler, K.-O. Velthaus, M. Ruckh, R. Laichinger, H.-W. Schock, D. Lincot, R. Ortega, and J. Vedel, *Proceedings of the 6th International Photovoltaic Science and Engineering Conference*, New Delhi, 10–14 February 1992 (Oxford & IBH, New Delhi, 1992).
- ²¹A. Loubat, M. Bouttemy, S. Gaiaschi, D. Aureau, M. Frégnaux, D. Mercier, J. Vigneron, P. Chapon, and A. Etcheberry, *Thin Solid Films* **633**, 87 (2017).
- ²²B. Dimmler and H. W. Schock, *Prog. Photovoltaics Res. Appl.* **4**, 425 (1996).
- ²³B. Canava, J. Vigneron, A. Etcheberry, J. F. Guillemoles, and D. Lincot, *Appl. Surf. Sci.* **202**, 8 (2002).
- ²⁴K. Ramanathan, F. S. Hasoon, S. Smith, D. L. Young, M. A. Contreras, P. K. Johnson, A. O. Pudov, and J. R. Sites, *J. Phys. Chem. Solids* **64**, 1495 (2003).
- ²⁵J. Lehmann, S. Lehmann, I. Laueremann, T. Rissom, C. A. Kaufmann, M. C. Lux-Steiner, M. Bär, and S. Sadewasser, *J. Appl. Phys.* **116**, 233502 (2014).
- ²⁶Copyright © ASTM International, West Conshohocken, PA. This practice is under the jurisdiction of ASTM Committee E-42 on Surface Analysis and is the direct responsibility of Subcommittee 42.03 on Auger Electron Spectroscopy and XPS. Current edition approved 15 September 1994. Published November 1994. Originally published as E 902–82. Last previous edition E 902–93.
- ²⁷S. Béchu, A. Loubat, M. Bouttemy, J. Vigneron, J.-L. Gentner, and A. Etcheberry, *Thin Solid Films* **669**, 425 (2019).
- ²⁸O. Roussel, M. Lamirand, N. Naghavi, J. F. Guillemoles, B. Canava, and A. Etcheberry, *Thin Solid Films* **515**, 6123 (2007).
- ²⁹M. Bouttemy et al., *Thin Solid Films* **519**, 7207 (2011).
- ³⁰J. F. Moulder, W. F. Stickle, P. E. Sobol, and K. D. Bomben, *Handbook of X-Ray Photoelectron Spectroscopy* (Physical Electronics, Norwalk, 1995).
- ³¹W. Calvet, B. Ümsür, A. Steigert, K. Prietzel, D. Greiner, C. A. Kaufmann, T. Unold, M. Lux-Steiner, and Iver Laueremann, *J. Vac. Sci. Technol. A* **37**, 031510 (2019).
- ³²M. Bär, I. Repins, M. A. Contreras, L. Weinhardt, R. Noufi, and C. Heske, *Appl. Phys. Lett.* **95**, 052106 (2009).
- ³³E. Handick et al., *ACS Appl. Mater. Interfaces* **9**, 3581 (2017).
- ³⁴F. I. Marín, *J. Electrochem. Soc.* **141**, 2409 (1994).
- ³⁵A. Etcheberry, H. Cachet, R. Cortes, and M. Froment, *Surf. Sci.* **482–485**, 954 (2001).
- ³⁶L. Kronik, D. Cahen, and H. W. Schock, *Adv. Mater.* **10**, 31 (1998).
- ³⁷J. F. Watts and J. Wolstenholme, *An Introduction to Surface Analysis by XPS and AES* (Wiley, Chichester, 2003).
- ³⁸J. A. Groenink and P. H. Janse, *Z. Phys. Chem.* **110**, 17 (1978).